https://doi.org/10.5194/nhess-2020-111
Preprint. Discussion started: 21 April 2020

Natural Hazards and Earth System Sciences
Open Access
Discussions

RAINFALL AND ROCKFALLS IN THE CANARY ISLANDS: ASSESSING A SEASONAL LINK

Massimo Melillo[a], Stefano Luigi Gariano[a], Silvia Peruccacci[a], Roberto Sarro[b], Rosa Marìa Mateos[c], Maria Teresa Brunetti[a]

[a] CNR IRPI, via Madonna Alta 126, 06128, Perugia, Italia
massimo.melillo@irpi.cnr.it, stefano.luigi.gariano@irpi.cnr.it, silvia.peruccacci@irpi.cnr.it

[b] IGME, c/ Alenza, 1, 28003, Madrid, España
r.sarro@igme.es

[c] IGME, Urb. Alcázar del Genil, 4. Edificio Zulema, bajos, 18006, Granada, España
rm.mateos@igme.es

Correspondence to: Maria Teresa Brunetti maria.teresa.brunetti@irpi.cnr.it

https://doi.org/10.5194/nhess-2020-111
Preprint. Discussion started: 21 April 2020

Natural Hazards and Earth System Sciences
Discussions

Abstract

Rockfalls are frequent and harmful phenomena occurring in mountain ranges, coastal cliffs and slope cuts. Albeit several natural processes concur in their formation and triggering, rainfall is one of the most common causes. The prediction of rock failures is of social significance for civil protection purposes and can rely on the statistical analysis of past rainfall conditions that caused the failures. The paper describes the analysis of information on rainfall-induced rockfalls in Gran Canaria and Tenerife, Canary Islands (Spain). An analysis of the monthly rainfall versus the monthly distribution of rockfalls reveals that they are correlated for most of the year, except in summer, when other triggers act to induce collapses. National and regional catalogues with hourly and daily rainfall measurements are used to reconstruct the cumulated amount (E) and the duration (D) of the rainfall responsible for the rock failures. Adopting a consolidated statistical approach, new ED rainfall thresholds for possible rockfall occurrence and the associated uncertainties are calculated for the two test sites. As far as is known, this is the first attempt to predict this type of failure using the threshold approach. Using the rainfall information, a map of the mean annual rainfall is obtained for Gran Canaria and Tenerife, and it is used to assess the differences between the thresholds. The results of is study are expected to improve the ability to forecast rockfalls in the Canary Islands, in view of implementing an early warning system to mitigate the rockfall hazard and reduce the associated risk.

Keywords: Rockfall, rainfall threshold, Canary Islands.

https://doi.org/10.5194/nhess-2020-111
Preprint. Discussion started: 21 April 2020

Natural Hazards and Earth System Sciences
Discussions

1 Introduction

Rockfalls are instability processes affecting mountainous regions, coastal cliffs and slope cuts. Being very rapid, they are extremely dangerous and life-threatening, especially when they occur in populated areas, along roads and railways. The most frequent triggering factors of rockfalls are rainfall, cycling thermal stress, and seismic activity (Wieckzorek and Jaeger, 1996; Keefer, 2002; Mateos, 2016; Ansari et al., 2015; Collins and Stock, 2016; Sarro et al., 2018; Saroglou, 2019). At regional and global scales, empirical approaches to forecast the occurrence of rockfalls may contribute reducing risk. Generally, for rainfall-induced slope failures the forecast can rely upon the definition of rainfall thresholds, i.e. the rainfall conditions that when reached or exceeded are likely to trigger the failure. Rainfall thresholds are calculated through the statistical analysis of historical rainfall conditions that have resulted in landslides (e.g., Guzzetti et al., 2007, 2008; Cepeda et al. 2010; Sengupta et al., 2010; Ruiz-Villanueva et al. 2011; Berti et al., 2012; Staley et al., 2013; Zêzere et al., 2015; Palenzuela et al., 2016; Rosi et al., 2016; Peruccacci et al., 2017; Segoni et al., 2018; Valenzuela et al., 2018, 2019). The definition of reliable empirical rainfall thresholds relies on the use of objective procedures for (i) the reconstruction of the rainfall events responsible for the failures and (ii) the calculation of the thresholds. For the purpose, Melillo et al. (2018) have proposed an algorithm that reconstructs rainfall events, identifies the rainfall conditions that have resulted in slope failures, and calculates probabilistic cumulated event rainfall-rainfall duration (*ED*) thresholds at different non-exceeding probabilities and their associated uncertainties (Peruccacci et al., 2012). The obtained thresholds are a set of parallel power-law curves in a log-log (*D*,*E*) plane, which are characterized by a slope and an intercept, the last being a function of the non-exceeding probability value (Brunetti et al., 2010).

In this work, a relationship between the amount of rainfall and the occurrence of rockfalls is assessed and empirical rainfall thresholds are defined for two test sites in Gran Canaria and Tenerife, Canary Islands (Spain). The possible prediction of rainfall-induced rock failures is of fundamental importance primarily for the safety of the inhabitants and for preserving infrastructures such as roads and buildings. An increasing level of safety against this type of hazard is also important for the local economy, one third of which is based on tourism. As far as is known, this is the first attempt to predict rock failures triggered by rain using the threshold approach. Recently, in Italy it has been observed that the slope of the power-law curve is dependent on the mean annual rainfall (MAR). In particular, the higher is the MAR the steeper is the threshold (Peruccacci et al., 2017). This relationship is explained assuming that where the landscape has been shaped over long time periods by landslides

https://doi.org/10.5194/nhess-2020-111
Preprint. Discussion started: 21 April 2020

triggered by a given minimum amount of rainfall, it is likely necessary at least as much rainfall to trigger the next landslides (Chen, 2015). For improving the discussion of the results, it has been considered worthwhile producing a map of the MAR for the islands of Gran Canaria and Tenerife using the available rainfall data sets.

The manuscript is organized as follows. After a description in Section 2 of the general settings of the two test sites, Section 3 describes the rainfall and rockfall datasets, and the methods used to determine *ED* rainfall thresholds and the map of the MAR. Section 4 illustrates in detail the relationship between the rainfall regime and the occurrence of rock failures, and presents the rainfall thresholds for the possible rockfall occurrence in the two test sites. Finally, in Section 5, the main findings of the work are summarised and discussed.

2 Test site description

The Canary Islands (Spain) are one of the major volcanic chain in the oceans. The archipelago consists of eight islands in the Atlantic Ocean, aligned along a W-SW to E-NE direction: El Hierro, La Palma, La Gomera, Tenerife, Gran Canaria, Fuerteventura, La Graciosa and Lanzarote. The geological origin of the Canary archipelago (800 km in length) is still under debate, but it has been traditionally interpreted as a hotspot track (Fullea et al., 2015).

The steep topography and the geological complexity of the archipelago influence the activation of an intense slope failures activity. Rockfalls are the most frequent landslide type in the Canary Islands, causing damage on built-up areas and communication networks.

Two test sites are selected for assessing the relationship between the rainfall and the occurrence of rockfalls. The first site (GC) is located in the north-western part of Gran Canaria island, and the second site (TEN) is the entire Tenerife island.

2.1 Gran Canaria Island (GC-200 road)

Gran Canaria is the third island in size of the Canarian archipelago. With an area of 1560 km^2 and a maximum altitude of 1956 m a.s.l., the island is approximately circular in shape (Fig. 1). The origin of Gran Canaria can be dated about 15 million years ago (Miocene) with the first submarine building stages of the Gran Canaria Volcano. From the geological point of view, the island presents the greatest variability of igneous rocks of the entire archipelago. Besides the distinctive lavas of the basanite basalt to trachyte phonolite series, Gran Canaria presents also other types of magma, such as tholeiitic

https://doi.org/10.5194/nhess-2020-111
Preprint. Discussion started: 21 April 2020

Natural Hazards and Earth System Sciences
Discussions

basalts and rhyolites (Troll and Carracedo, 2016). Massive flank failures and erosion give place to chaotic deposits that cover large areas.

The test site is the GC-200 road located in the north-western extreme of Gran Canaria, and specifically between the localities of Agaete and Aldea. The road constitutes the main transportation corridor between the two localities. With a length of 34 km, the road path is very tortuous following the contour of the coast, a very step coastline with some of the highest cliffs in Europe. The road has heavy traffic estimated on average at 1500 vehicles per day. The geology of the test site area is within the domain of the basaltic shield stage, Middle Miocene in age. Along the road, an alternance of alkaline basaltic deposits and piroclastic flows can be observed. In some parts, gravitational deposits (mainly colluvial) also outcrop covering wide areas.

Regarding climatological conditions, Gran Canaria is located in a transitional zone between temperate and tropical conditions. The conical morphology of Gran Canaria retains the humidity of the predominant N-NE trade winds of the subtropical Azores anticyclone on the north side of the island. As a result, the northern flanks are humid and vegetation is vigorous, while the south part of the island is very dry and the conditions are very arid and desert-like. Annual rainfall ranges between 100 and 1000 mm on average, increasing with altitude. In the test site the climate is very dry, with low average annual rainfall (< 100 mm) and high average annual temperature (~ 20°C).

2.2 Tenerife island

Tenerife (Fig. 1) is the largest (2057 km^2) and the most populated (950,000 inhabitants and 13.2 million visitors in 2019) island of the archipelago. It is home to the third largest volcano in the world (Pico del Teide, 3718 m a.s.l.).

From a geological point of view, Tenerife was constructed via Miocene–Pliocene shields that now form the vertices of the island. The shields were unified into a single edifice by later volcanism that continued in central Tenerife from approximately 12 to 8 million years ago and was followed by a period of dormancy. Rejuvenation at approximately 3.5 Ma is recorded by the central Las Cañadas Volcano, and long residence times of magmas during this period favoured magmatic differentiation processes to produce an episode of felsic and highly explosive felsic volcanism (Troll and Carracedo, 2016).

The steep orography of the island and the climate variety have resulted in a diversity of landscapes and geographical formations. Very impressive coastal cliffs (till 500 m in height) are present in the

https://doi.org/10.5194/nhess-2020-111
Preprint. Discussion started: 21 April 2020

northern corner of Tenerife. This area is also characterized by narrow and deep ravines which determine an intense slope activity.

The climate of Tenerife is subtropical oceanic; the minimum and maximum annual average temperatures are about 15ºC in winter and 24ºC in summer. Tenerife offers a large variety of micro-climate zones controlled by the altitude and the winds.

3 Data and methods

The availability of rainfall measurements and landslide information is fundamental to define reliable rainfall thresholds. For the selection of the rain gauges, the data quality and the location of the rain gauges are assessed, given that these features are crucial to characterize the spatial-temporal variation of the precipitations. Similarly, the calculation of the MAR relies on the availability of sufficiently long rainfall series (at least 30 years). This is difficult to achieve for a dense network of rain gauges, where sensors may exhibit different operating time periods. The World Meteorological Organization (WMO) guidelines on the calculation of the annual standard normal, specifically the MAR, recommend at least 10 years to define at least provisional MAR maps (WMO, 1989). This is the case in the test sites, where a lot of rainfall information is limited to short time periods (the average is 15.6 years), thus hampering the calculation of the MAR with a detailed space resolution.

3.1 Rainfall data

In the GC test site, hourly rainfall data (purple triangles in Fig. 1) from the Spanish National Meteorological Service (AEMET) network (in total 25 stations among which 4 are close to the study area) are used for the calculation of rainfall thresholds. Moreover, daily rainfall data (orange triangles in Fig.1) are provided from the *Consejo Insular de Aguas de Gran Canaria* (CIAGC) regional rain gauge network (13 stations) and from AEMET (92 stations, among which 7 are close to the study area). Some of the sensors of the AEMET network provide both hourly and daily rainfall, in different time periods. Details of the rainfall series are reported in Table 1.

For the TEN test site, rainfall measurements are provided by AEMET with the contribution of regional networks. As for the GC test site, the rainfall analysis is performed using both hourly and daily data. The two networks in the TEN test site are composed by 34 rain gauges recording hourly data (purple triangles in Fig. 1) and 66 rain gauges recording daily data (orange triangles in Fig. 1).

https://doi.org/10.5194/nhess-2020-111
Preprint. Discussion started: 21 April 2020

To calculate the MAR for the two test sites, yearly and monthly rainfall data provided by AEMET and by *Sistema de Información Agroclimático y de Regadíos* (SIAR), respectively, are used (Table 1). In particular, in order to obtain homogeneous maps, data recorded in the 20-year period from January 2000 to December 2019 in both test sites are selected. Following WMO guidelines (WMO, 1989), only stations with at least 10 years of data are included in the analysis. Overall, 72 (one every 22 km^2) and 67 (one every 31 km^2) rain gauges are used to calculate MAR in Gran Canaria and Tenerife, respectively. The average number of sensors operating per year in the considered period is 56 (84%; one every 28 km^2) in Grand Canaria and 47 (65%; one every 43 km^2) in Tenerife. The used rain gauges are homogeneously distributed over the test site areas.

Using the monthly and annual rainfall data recorded by the 103 rain gauges in the two islands, the MAR for the period 2000-2019 was calculated for each station. Moreover, the coefficient of variation of the MAR is calculated by dividing its standard deviation by the MAR. This coefficient represents the variability of the MAR in the considered time interval. The map of the MAR and of its coefficient of variation are calculated using the tension spline tool in ESRI ArcMAP 10.7.1.

3.2 Rockfall data

The information on the rockfalls was collected by the Canarian Civil Protection Authorities in the TEN test site and by the Road Maintenance Service in the GC test site. In particular, for the GC test site a total of 8174 rockfall events occurred from January 2010 to March 2016 was documented. A catalogue was prepared defining accurately the location of each impact along the road using orthophotos available for the region and technical reports. The information for each event includes kilometre point, number of events, date, and boulder size. In GC only 535 rockfalls characterized by medium to large size are included in the analysis for the thresholds, whereas small and very small rockfalls (< 10^{-3} m^3) are discarded. Analogously, a catalogue of 1898 rockfalls that impacted along Tenerife roads from January 2010 to November 2017 was prepared. For each event, the information includes rockfall localization, geographic accuracy, occurrence day, month, year, and time (if available), and temporal accuracy.

The influence of the rainfall on the occurrence of rockfalls is assessed analysing the distribution of monthly rainfall (Figs. 2a,b) and monthly number of rockfalls (Figs. 2c,d) on the two test sites. As expected, an increase of the rainfall in the autumn-winter period, between October and March, is observed in both islands, with a maximum in November.

https://doi.org/10.5194/nhess-2020-111
Preprint. Discussion started: 21 April 2020

The monthly distribution of rockfalls in Gran Canaria (Fig. 2c) is coherent with the rainfall values in the period January-April, with a maximum in February (~ 130; Fig. 2a). For the remaining dry (May to September) and wet (October to December) months the number of rock failures decreases and becomes almost flat (below 50). This behaviour suggests the presence of triggering mechanisms other than the rainfall. For the TEN test site, the number of rockfalls per month (Fig. 2b) is similar to the rainfall distribution, confirming anyway the presence of one or more additional triggers as evidenced by the abundance of failures between May and September (Fig. 2d) when the rainfall is irrelevant.

3.3 Empirical rainfall thresholds

Empirical *ED* thresholds are represented by the following power law curve:

$$E = (\alpha \pm \Delta\alpha) \times D^{(\gamma \pm \Delta\gamma)} \quad (1)$$

where E is the cumulated event rainfall (in mm), D is the duration of the rainfall event (in hours or in days), α and γ are the intercept and the slope of the curve, respectively, and $\Delta\alpha$ and $\Delta\gamma$ are the uncertainties associated with them. Thresholds at different non-exceedance probabilities are calculated adopting the frequentist approach and the bootstrap nonparametric statistical technique (Brunetti et al., 2010; Peruccacci et al., 2012), using 5000 randomly selected synthetic series of *DE* pairs. A threshold at 5% non-exceedance probability should leave 5% of the empirical *DE* pairs below itself. The parameter uncertainties depend mostly on the number and the distribution of the rainfall conditions. The minimum number of *DE* pairs needed for having stable mean values of the parameters α and γ (i.e. reliable thresholds) depends on the distribution and dispersion of the empirical data points in the *DE* domain.

3.4 The CTRL-T algorithm for threshold calculation

The quantitative identification of the rainfall responsible for slope failures and the definition of reliable thresholds are fundamental steps towards a well-founded event prediction (Peruccacci et al., 2017; Melillo et al., 2018). The use of standardized procedures for the reconstruction of the rainfall conditions able to trigger past failures and for the definition of thresholds is necessary for enhancing the objectivity and reproducibility of the curves. The tool named CTRL-T (Calculation of Thresholds for Rainfall-induced Landslides - Tool) proposed by Melillo et al. (2018) is exploited to calculate *ED* thresholds for the two test sites. CTRL-T reconstructs rainfall events starting from continuous rainfall series. For each rockfall, the algorithm: 1) identifies automatically the representative rain gauge; 2) identifies multiple (D,E) rainfall conditions responsible for the failure; 3) selects among them the

https://doi.org/10.5194/nhess-2020-111
Preprint. Discussion started: 21 April 2020

maximum probability rainfall conditions (MPRCs). Then, analysing the distribution of the MPRCs it calculates probabilistic rainfall thresholds at different non-exceeding probabilities and their associated uncertainties. In order to avoid using wrong temporal information (i.e., incorrect dates for the occurrence of rockfalls) in the definition of the thresholds, the rainfall conditions having a delay longer than 48 hours between the rainfall ending time and the rockfall occurrence are discarded.

Using CTRL-T, 82 rockfalls occurred between 2012 and 2016 in GC test site and 626 rockfalls occurred between 2010 and 2016 in the TEN test site are selected (light green dots in Fig. 2). The remaining records are discarded due to the: 1) absence of rainfall data in the period including the collapse occurrence time; 2) absence of rain gauges within a buffer of 15 km radius centred on the rockfall; 3) lack of an evident correlation with the rainfall. The definition of rainfall thresholds relies only upon rainfall conditions that triggered the first failure in each event. As a consequence, numerous rockfalls (106, 39% in GC and 271, 30% in TEN) which occurred at the same date and in the same location, and which are associated with the same rainfall event are discarded. In GC among the remaining rockfalls 53 are analysed with daily and 29 with hourly rainfall data, respectively. The low number of rock failures associated to hourly-based rain gauges is to be ascribed to the low density of the sensors in the area. In TEN 245 rockfalls are reconstructed with hourly data and 381 with daily rainfall data. Note that for 83 failures it was possible reconstructing the rainfall conditions using sensors from both the two rain gauge networks. As a consequence, the reconstructed (D,E) rainfall conditions have different temporal resolutions and are used to define both hourly-based and daily-based rainfall thresholds.

4 Results

A correlation between the rainfall and the observed failures is confirmed by the comparison between the monthly rainfall and the corresponding number of rockfalls both in GC and in TEN (Fig. 3). Figures 3a,b,c show the boxplots of cumulated monthly rainfall based on the data recorded in rain gauges used to reconstruct the rainfall responsible for rockfalls for GC and TEN test sites. Inspection of these figures reveals that the rainfall pattern in the two test sites is typically Mediterranean, with a maximum in winter (but also in October and November) and a minimum in summer, with practically no rain in the warmest months. Analysing data from seven daily-based rain gauges in GC (GC-d), it turns out that the rainiest months are February and November with an average rainfall of 52.2 mm and 55.7 mm, a highest rainfall of 98.6 mm and 133.9 mm, and a median rainfall of 42.3 mm and 39.8 mm, respectively (Fig. 3a). A similar trend is found for Tenerife using both daily and hourly data. Data from 40 daily-based rain gauges in TEN (TEN-d) are analysed finding an average rainfall

https://doi.org/10.5194/nhess-2020-111
Preprint. Discussion started: 21 April 2020

of 64.6 mm and 86.4 mm, a highest rainfall of 183.5 mm and 183.6 mm, and a median rainfall of 56.1 mm and 93.2 mm for February and November, respectively (Fig. 3b). Data from 21 hourly-based rain gauges in TEN (TEN-h) are analysed finding an average rainfall of 88.8 mm and 82.0 mm, a highest rainfall of 169.8 mm and 190.8 mm, and a median rainfall of 97.5 mm and 66.4 mm for February and November, respectively (Fig. 3c).

Figures 3d,e,f portray the monthly number of rockfalls associated with rainfall events for GC-d, TEN-d and TEN-h. The GC catalogue lists 53 collapses occurred in the period from November 2012 to October 2016, with the majority of the failures in 2015 (22). The month with the largest number of rockfalls (14) is February, followed by January (8) and November (7). The least number of failures is reported in September (1) and no rainfall-induced rockfalls are reported in May and July (Fig. 3d). The 245 rock failures in the TEN-d catalogue cover the period from September 2010 to February 2016, with the majority of records in 2014 (66). The month with the largest number of rockfalls (80) is November, followed by October (37) and December (36). The least number of failures is reported in May (1) and no rainfall-induced rockfalls are reported in June and July (Fig. 3e). The TEN-h catalogue lists 381 rockfalls occurred in the period from September 2010 to November 2016, with the majority of the failures in 2014 (90). The month with the largest number of rockfalls (115) is November, followed by December (72) and October (64). The least number of failures is reported in May (1) and no collapses are reported in July (Fig. 3f).

The rainfall that triggered the rockfalls is classified according to the method proposed by Alpert et al. (2002), based on six daily rainfall (E_d) categories from “light” to “torrential” over the Mediterranean (Table 2). Using the procedure adopted by Melillo et al. (2016), each rainfall condition responsible for rock failures (MPRC) is attributed to a specific category. In particular, for events lasting less than 24 hours, a category based on the total cumulated rainfall of the event is assigned. For events lasting more than 24 hours, the maximum value of the cumulated rainfall in 24 hours in a moving window is used. In GC, over 40% of the MPRCs responsible for the collapses are classified as moderate-high (MH); in TEN, approximately 30% as high (H) and high-torrential (HT). No MPRCs are found in the lowest Alpert’s category (light, Table 2). Figures 3g,h,i show the cumulated percentage of rainfall events per month grouped according to Alpert’s classification. In GC-d, in February (Fig. 3g) 6 rockfalls (43%) are triggered by a rainfall classified as H, 3 (21%) as torrential (H), 3 (22%) as MH, and 1 as light-moderate (LM) and HT each (14%). In TEN-d, in November, 29 rockfalls (36%) are triggered by a rainfall classified as HT, 26 (33%) as MH, 22 (28%) as H, 2 (2%) as LM, and 1 (1%) as T (Fig. 3h). In TEN-h, in November, 5 (4%), 26 (23%), 26 (23%), 31 (27%) and 27 (23%) rockfall are triggered by a rainfall classified as LM, MH, H, HT and T, respectively (Fig. 3i).

https://doi.org/10.5194/nhess-2020-111
Preprint. Discussion started: 21 April 2020

Using the catalogues of rainfall events with rockfalls described above and the CTRL-T tool, *ED* thresholds, and their associated uncertainties are calculated for GC and TEN test sites. Table 3 lists the number of MPRC used to define the thresholds, the equations of the power law curves, and the range of validity for the thresholds, expressed in hours or days. Note that *D* must be expressed in days in the equations for the thresholds calculated with daily data, and in hours in the equations for the thresholds calculated with hourly data (Gariano et al., 2020).

Figure 4a shows, in logarithmic coordinates, the distribution of the (*D*,*E*) rainfall conditions, reconstructed with daily data, that have caused rockfalls in GC (53 blue dots) and in TEN (245 green dots). In particular, the 53 daily rainfall conditions responsible for the rockfalls in GC have durations in the range $1 \leq D \leq 11$ days (with an average value of 2 days) and cumulated rainfall in the range $16.5 \leq E \leq 219.9$ mm (average value 51.6 mm). All the conditions were recorded in rain gauges located at a maximum distance of 5.7 km from the failures, with a mean value of 2.8 km. The 245 daily-based rainfall conditions associated with the collapses in TEN have durations ranging from one to 15 days, with a mean value of two days. The cumulated rainfall ranges from 15.4 to 235.0 mm, with an average of 71.5 mm. The average distance between the rockfalls and their representative rain gauges is 2.2 km, with a maximum distance of 5 km. Figure 4a portrays also the 5% *ED* thresholds for GC ($T_{5,GC\text{-}d}$, blue curve) and TEN ($T_{5,TEN\text{-}d}$, green curve). The shaded areas around the threshold lines show the uncertainty regions associated to the thresholds (Table 3). Figure 5b portrays the same $T_{5,GC\text{-}d}$ and $T_{5,TEN\text{-}d}$, in linear coordinates, in the range $1 \leq D \leq 7$ days.

Figure 4c shows, in logarithmic coordinates, the distribution of the (*D*,*E*) rainfall conditions, reconstructed with hourly data, that have triggered rock failures in TEN (381 purple dots). The hourly rainfall conditions associated to rockfalls have durations ranging from 2 to 712 hours and mean value of 111 hours. The cumulated rainfall ranges from 10.6 to 433.9 mm, with an average of 105.6 mm. The average distance between the rockfalls and the representative rain gauges is 6.7 km, with a maximum distance of 14.9 km. In the log-log plot the purple curve is the 5% threshold for TEN ($T_{5,TEN\text{-}h}$) obtained with hourly data. Figure 5d portrays the same $T_{5,TEN\text{-}h}$, in linear coordinates, in the range $1 \leq D \leq 120$ hours. The uncertainty associated with the threshold (purple shaded area in Figs. 4c,d) is also shown.

The difference between the $T_{5,GC\text{-}d}$ and $T_{5,TEN\text{-}d}$ thresholds can be ascribed to the different MAR in the two test sites. Figure 5 portrays the maps of the MAR and of its coefficient of variation, which is the percentual variability (standard deviation) of the MAR in the considered time interval. The geographical distribution of the MAR values exhibits the highest values in the northern parts of both

https://doi.org/10.5194/nhess-2020-111
Preprint. Discussion started: 21 April 2020

islands, where it overcomes 800 mm (Fig. 5a). On the contrary, the highest values of the coefficient of variation (i.e. an index of the MAR variability) are localized in the southern part of the islands, where the rain gauge density is lower (Fig. 5b).

5 Discussion and conclusions

In Canary Island rainfall is the most important triggering factor for rockfalls (Fig. 2). Nevertheless, there are other factors that predispose directly or indirectly the trigger of the failure (Temiño et al., 2013a). Factors that greatly accentuate this hazard in the two test sites are wind, geomorphological characteristics (e.g., slope, aspect), type of soil and seismic activity. Regarding the wind many collapses are caused by strong gusts of wind that affect the northern side of Tenerife Island and the road GC-200 from Agaete to Aldea in Gran Canaria. (Temiño et al., 2013b). Regarding the geomorphology, the existence of many sections of road running through the old basaltic massifs with significant sub-vertical jointing, makes the area very susceptible to rock failures. In addition, the action of the trade winds on the higher altitude areas, produces an increase in the relative humidity, as large masses of water vapor are retained by steep slopes resulting in an intense weathering (and weakening) of the rock masses. Finally, the large flank instability of the two test sites (especially in the northwest sector of the Gran Canaria island) could be related to structural control and to seismic activity connected to the dynamic geologic condition that characterizes them. (Masson et al., 2002; Temiño et al. 2013b; Urgeles et al., 2001).

By selecting the subset of rockfalls triggered by rainfall it can be observed that their monthly frequency is linked to the monthly distribution of the rainfall measured in nearby rain gauges (Figs. 3a-f). For GC-d (Figs. 3a,d) the correlation is apparently weaker in fall than in winter, but this could be ascribed to a statistical fluctuation and should be confirmed by increasing the number of events. Conversely, for TEN-d (Figs. 3b,e) the monthly number of rock failures well reflects the monthly rainfall amount, suggesting that rainfall is the only triggering cause. Hourly rainfall data in TEN-h (Figs. 3c,f) confirm partially this outcome, since even with a median lower amount of rainfall, a higher number of rock failures is expected to occur from October to December than in February.

The number of rockfalls for which it has been possible to reconstruct the rainfall conditions (MPRCs) using daily and hourly data in the TEN test site (Figs. 3e,f) is different. This is mostly due to the worst temporal resolution of the TEN-d dataset.

https://doi.org/10.5194/nhess-2020-111
Preprint. Discussion started: 21 April 2020

In the two test sites, the majority of the rainfall responsible for rockfalls belongs to the Alpert's MH category (Figs. 3g,i). In TEN-h, 31 events belong to the most severe category T, whereas in TEN-d only one event is found in the T category. This result could be ascribed to the time step of the moving window used to assign the Alpert's category. For a rainfall event lasting more than one day, the Alpert's category varies depending on the data temporal resolution, since the time step is one hour or one day for the hourly and daily data, respectively. In TEN-d, the total amount of rainfall responsible for the failure is shared in two or more consecutive days, causing a lowering of the Alpert's category, as confirmed by the paucity of T events in TEN-d.

Figure 4 shows that $T_{5,TEN\text{-}d}$ is higher and steeper than $T_{5,GC\text{-}d}$. This means that, at increasing values of *D*, a smaller amount of rainfall (*E*) is necessary to trigger the collapses in GC than in TEN. Comparing Figures 1 and 5, the recorded rockfalls in the TEN test site are localized in areas including several classes of MAR (ranging from 100 to 800 mm), while in GC test site they fall in the area characterized by the lowest class of MAR ($\leq$ 100 mm). The different ranges of MAR values in the two test sites are able to explain the observed differences in the two daily *ED* thresholds (Fig. 4a). This finding confirms that where the MAR is higher, the minimum rainfall conditions able to trigger a failure, specifically a rockfall, are also higher.

Moreover, the threshold defined for the TEN test site has an uncertainty smaller than the threshold for GC test site. Peruccacci et al. (2012) observed that the parameter uncertainty reduces as the number of MPRC used to calculate the threshold increases. In particular, as derived from Table 3, the relative uncertainty of the intercept, $\Delta\alpha/\alpha$ is 9.8% for $T_{5,GC\text{-}d}$ and 4.9% for $T_{5,TEN\text{-}d}$. Regarding the slope of the curves, $\Delta\gamma/\gamma$ is 16.1% for $T_{5,GC\text{-}d}$ and 6.7% for $T_{5,TEN\text{-}d}$. Given the lower uncertainty range and relative uncertainties of both parameters, $T_{5,TEN\text{-}d}$ has a reliability higher than that of $T_{5,GC\text{-}d}$. The same analysis for the $T_{5,TEN\text{-}h}$ threshold gives $\Delta\alpha/\alpha$ = 9.3% and $\Delta\gamma/\gamma$ = 4.2. Thresholds with an hourly temporal resolution and having relative uncertainties of the parameters α and γ lower than 10% could be implemented in an operative system for the prediction of rainfall-induced failures (Peruccacci et al., 2012; 2017). The thresholds for different non-exceedance probabilities obtained for TEN test site using hourly rainfall data are suited for the design of probabilistic schemes for the operative prediction of rainfall-induced rockfalls. An improvement in the number of rain gauges providing hourly measurements, as well as in the number of recorded rock failures, would be necessary in GC test site in order to reduce the uncertainty of the threshold.

Currently, neither prototype nor operative early warning systems for rainfall-induced failures are present in the Canary Islands (Guzzetti et al. 2020). The findings of this work can contribute to the understanding of the rainfall conditions that can trigger rainfall-induced rockfalls in Tenerife and in the western part of Gran Canaria, and their relationship with mean annual rainfall regime. These findings have scientific and social implications given that in both test sites also spring and autumn are characterized by a moderately occurrence of rock failures, with relevant impacts on the population, tourism activities, and local economy. As long as a sufficient amount of empirical data will be available in both test sites (and also in other islands of the archipelago), the method adopted in this work for the definition of reliable rainfall thresholds can be replicated, and the results can be implemented in a prototype early warning system.

6 Acknowledgements

Research conducted within the framework of the U-Geohaz project (Geohazard Impact Assessment for Urban Areas) funded by the European Commission, Directorate-General Humanitarian Aid and Civil Protection (ECHO), under the call UCPM-2017-PP-AG. This work was also funded by the Salvador de Madariaga Mobility Program from the Spanish Ministry of Science, Project: PRX18/00020.

7 References

Alpert, P., Ben-Gai, T., Baharan, A., Benjamini, Y., Yekutieli, D., Colacino, M., Diodato, L., Ramis, C., Homar, V., Romero, R., Michaelides, S., and Manes, A.: The paradoxical increase of Mediterranean extreme daily rainfall in spite of decrease in total values, Geophy. Res. Lett., 29(11), 31-1–31-4, https://doi.org/10.1029/2001GL013554, 2012.

Ansari, M.K., Ahmed, M., Rajesh Singh, T.N., and Ghalayani, I.: Rainfall, a major cause for rockfall hazard along the roadways, highways and railways on hilly terrains in India, in: Lollino, G., Manconi, A., Clague, J., Shan, W., and Chiarle, M. (Eds.) Engineering Geology for Society and Territory – Vol. 1, pp. 457–460, Springer, Cham, https://doi.org/10.1007/978-3-319-09300-0_87, 2015.

Berti, M., Martina, M.L.V., Franceschini, S., Pignone, S., Simoni, A., and Pizziolo, M.: Probabilistic rainfall thresholds for landslide occurrence using a Bayesian approach, J. Geophys. Res, 117, F04006, https://doi.org/10.1029/2012JF002367, 2012.

Brunetti, M.T., Peruccacci, S., Rossi, M., Luciani, S., Valigi, D., and Guzzetti, F.: Rainfall thresholds for the possible occurrence of landslides in Italy, Nat. Hazards Earth Syst. Sci., 10, 447–458, https://doi.org/10.5194/nhess-10-447-2010, 2010.

https://doi.org/10.5194/nhess-2020-111
Preprint. Discussion started: 21 April 2020

Natural Hazards and Earth System Sciences
Discussions

Cepeda, J., Höeg, K., and Nadim, F.: Landslide-triggering rainfall thresholds: a conceptual framework, Q. J. Eng. Geol. Hydroge., 43, 69–84, https://doi.org/10.1144/1470-9236/08-066, 2010.

Chen, C., Saito, H., and Oguchi, T.: Rainfall intensity–duration conditions for mass movements in Taiwan, Prog. Earth Planet. Sci., 2, 14, https://doi.org/10.1186/s40645-015-0049-2, 2015.

Collins, B.D., and Stock, G.M.: Rockfall triggering by cyclic thermal stressing of exfoliation fractures. Nat. Geosci., 9, 395–400, https://doi.org/10.1038/ngeo2686, 2016.

Fullea, J., Camacho, A.G., Negredo, A.M., and Fernández, J.: The Canary Islands hot spot: new insights from 3D coupled geophysical–petrological modelling of the lithosphere and uppermost mantle, Earth Planet. Sci. Lett., 409, 71–88, https://doi.org/10.1016/j.epsl.2014.10.038, 2015.

Gariano, S.L., Melillo, M., Peruccacci, S., and Brunetti, M.T.: How much does the rainfall temporal resolution affect rainfall thresholds for landslide triggering?, Nat. Hazards, 100, 655–670, https://doi.org/10.1007/s11069-019-03830-x, 2020.

Guzzetti, F., Peruccacci, S., Rossi, M., and Stark, C.P.: Rainfall thresholds for the initiation of landslides in central and southern Europe, Meteorol. Atmos. Phys., 98(3), 239–267, https://doi.org/10.1007/s00703-007-0262-7, 2007.

Guzzetti, F., Peruccacci, S., Rossi, M., and Stark, C.P.: The rainfall intensity–duration control of shallow landslides and debris flows: an update, Landslides 5(1), 3–17, https://doi.org/10.1007/s10346-007-0112-1, 2008.

Guzzetti, F., Gariano, S.L., Peruccacci, S., Brunetti, M.T., Marchesini, I., Rossi, M., and Melillo, M.: Geographical landslide early warning systems, Earth-Sci. Rev., 200, 102973, https://doi.org/10.1016/j.earscirev.2019.102973, 2020.

Keefer, D.K.: Investigating landslides caused by earthquakes – A historical review, Surv. Geophys., 23, 473–510, https://doi.org/10.1023/A:1021274710840, 2002.

Masson, D.G., Watts, A.B., Gee, M.J.R., Urgeles, R., Mitchell, N.C., Le Bas, T.P., and Canals, M.: Slope failures on the flanks of the western Canary Islands, Earth-Sci. Rev., 57, 1–35, https://doi.org/10.1016/S0012-8252(01)00069-1, 2002.

Mateos, R.M., García-Moreno, I., Reichenbach, P., Herrera, G., Sarro, R., Rius, J., and Aguiló, R.: Calibration and validation of rockfall modelling at regional scale: application along a roadway in

https://doi.org/10.5194/nhess-2020-111
Preprint. Discussion started: 21 April 2020

Mallorca (Spain) and organization of its management, Landslides, 13, 751-763, https://doi.org/10.1007/s10346-015-0602-5, 2016.

Melillo, M., Brunetti, M.T., Peruccacci, S., Gariano, S.L., and Guzzetti, F.: Rainfall thresholds for the possible landslide occurrence in Sicily (southern Italy) based on the automatic reconstruction of rainfall events, Landslides, 13(1), 165–172, https://doi.org/10.1007/s10346-015-0630-1, 2016.

Melillo, M., Brunetti, M.T., Peruccacci, S., Gariano, S.L., Roccati, A., and Guzzetti, F.: A tool for the automatic calculation of rainfall thresholds for landslide occurrence, Environ. Model. Softw., 105, 230–243, https://doi.org/10.1016/j.envsoft.2018.03.024, 2018.

Palenzuela, J.A., Jiménez-Perálvarez, J.D., and Chacón, J.: Assessing critical rainfall thresholds for landslide triggering by generating additional information from a reduced database: an approach with examples from the Betic Cordillera (Spain), Nat. Hazards, 84, 185–212, https://doi.org/10.1007/s11069-016-2416-8, 2016.

Peruccacci, S., Brunetti, M.T., Luciani, S., Vennari, C., and Guzzetti, F.: Lithological and seasonal control of rainfall thresholds for the possible initiation of landslides in central Italy, Geomorphology, 139–140, 79–90, https://doi.org/10.1016/j.geomorph.2011.10.005, 2012.

Peruccacci, S., Brunetti, M.T., Gariano, S.L., Melillo, M., Rossi, M., and Guzzetti, F.: Rainfall thresholds for possible landslide occurrence in Italy, Geomorphology, 290, 39–57, https://doi.org/10.1016/j.geomorph.2017.03.031, 2017.

Rosi, A., Peternel, T., Jemec-Auflič, M., Komac, M., Segoni, S., and Casagli, N.: Rainfall thresholds for rainfall-induced landslides in Slovenia, Landslides, 13, 1571–1577, https://doi.org/10.1007/s10346-016-0733-3, 2016.

Ruiz-Villanueva, V., Bodoque, J.M., Díez-Herrero, A., and Calvo, C.: Triggering threshold precipitation and soil hydrological characteristics of shallow landslides in granitic landscapes, Geomorphology, 133(3), 178–189, https://doi.org/10.1016/j.geomorph.2011.05.018, 2011.

Saroglou, C.: GIS-based rockfall susceptibility zoning in Greece, Geosciences, 9(4), 163, https://doi.org/10.3390/geosciences9040163, 2019.

Sarro, R., Riquelme, A., García-Davalillo, J., Mateos, R., Tomás, R., and Pastor, J.: Rockfall Simulation Based on UAV Photogrammetry Data Obtained during an Emergency Declaration:

https://doi.org/10.5194/nhess-2020-111
Preprint. Discussion started: 21 April 2020

Application at a Cultural Heritage Site, Remote Sens., 10(12), 1923, https://doi.org/10.3390/rs10121923, 2108.

Segoni, S., Piciullo, L., and Gariano, S.L.: A review of the recent literature on rainfall thresholds for landslide occurrence, Landslides, 15, 1483–1501, https://doi.org/10.1007/s1034 6-018-0966-4, 2018.

Sengupta, A., Gupta, S., and Anbarasu, K.: Rainfall thresholds for the initiation of landslide at Lanta Khola in north Sikkim, India, Nat. Hazards, 52, 31–42, https://doi.org/10.1007/s11069-009-9352-9, 2010.

Staley, D.M., Kean, J.W., Cannon, S.H., Schmidt, K.M., and Laber, J.L.: Objective definition of rainfall intensity–duration thresholds for the initiation of post-fire debris flows in southern California, Landslides, 10, 547–562, https://doi.org/10.1007/s10346-012-0341-9, 2013.

Temiño, J.Y., Rodrìguez-Peces, M.J., Marchesini, S., Leyva, S., and Dìaz-Hernàndez, J.L.: Amplification of the destructive effects of rock falls by sliding on volcanic soils: examples from the Anaga Massif (Tenerife Island, Spain), in: Margottini, C., Canuti, P., and Sassa, K. (Eds.) Landslide Science and Practice, Springer-Verlag Berlin Heidelberg, Vol. 1, pp. 191–195, https://doi.org/10.1007/978-3-642-31325-7_25, 2013a.

Temiño, J.Y., Rodrìguez-Peces, M.J., Sànchez, N., Galindo, I., and del Potro, R.: Geomorphologic evidences of flank instabilities in the eastern sector of the Tejeda volcano (Canary Islands, Spain) during the Quaternary, in: Margottini, C., Canuti, P., and Sassa, K. (Eds.) Landslide Science and Practice, Springer-Verlag Berlin Heidelberg, Vol. 7, pp. 65–72, https://doi.org/10.1007/978-3-642-31313-4_9, 2013b.

Troll, V.R., and Carracedo, J.C.: The Geology of the Canary Islands, Elsevier, pp. 636. ISBN 978-0-12-809663-5, https://doi.org/10.1016/C2015-0-04268-X, 2016.

Urgeles, R., Canals, M., and Masson, D.G.: 2001 Flank stability and processes off the western Canary Islands: a review from El Hierro and La Palma, Sci. Mar., 65(1), 21–31, https://doi.org/10.3989/scimar.2001.65s121, 2001.

Valenzuela, P., Domínguez-Cuesta, M.J., Mora García, M.A., and Jiménez-Sánchez, M.: Rainfall thresholds for the triggering of landslides considering previous soil moisture conditions (Asturias, NW Spain), Landslides, 15, 273–282, https://doi.org/10.1007/s10346-017-0878-8, 2018.

Valenzuela, P., Zêzere, J.L., Domínguez-Cuesta, M.J., and Mora García, M.A.: Empirical rainfall thresholds for the triggering of landslides in Asturias (NW Spain), Landslides, 16, 1285–1300, https://doi.org/10.1007/s10346-019-01170-2, 2019.

Wieczorek, G.F., and Jaeger, S.: Triggering mechanisms and depositional rates of postglacial slope movement processes in the Yosemite Valley, California, Geomorphology, 15, 17–31, https://doi.org/10.1016/0169-555X(95)00112-I, 1996.

WMO – World Meteorological Organization: Calculation of Monthly and Annual 30-Year Standard Normals, WMO/TD No. 341, WCDP-No. 10, Geneva, 1989.

Zêzere, J.L., Vaz, T., Pereira, S., Oliveira, S.C., Marques, R., and Garcia, R.A.C.: Rainfall thresholds for landslide activity in Portugal: a state of the art, Environ. Earth Sci., 73(6), 2917–2936, https://doi.org/10.1007/s12665-014-3672-0, 2015.

https://doi.org/10.5194/nhess-2020-111
Preprint. Discussion started: 21 April 2020

496 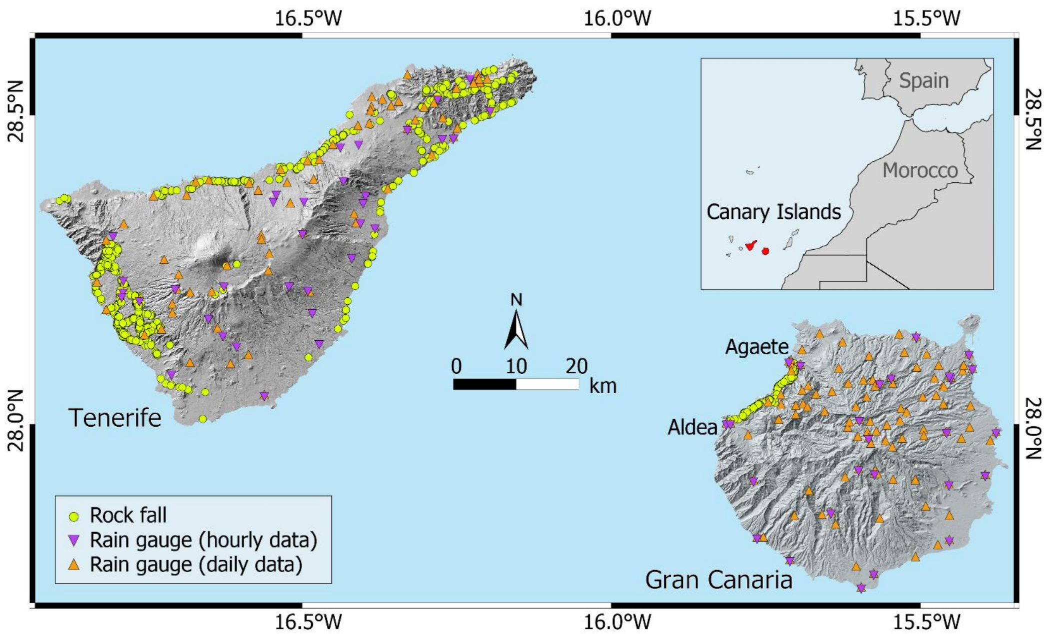

497 Figure 1. GC and TEN test sites. Location of the rain gauges providing hourly (purple triangles) and daily
498 (orange triangles) rainfall measurements, and of rockfalls used for threshold calculations (light green dots).
499 Hillshade derived from MDT05 2009 CC-BY 4.0 scne.es.

https://doi.org/10.5194/nhess-2020-111
Preprint. Discussion started: 21 April 2020

Natural Hazards and Earth System Sciences
Discussions

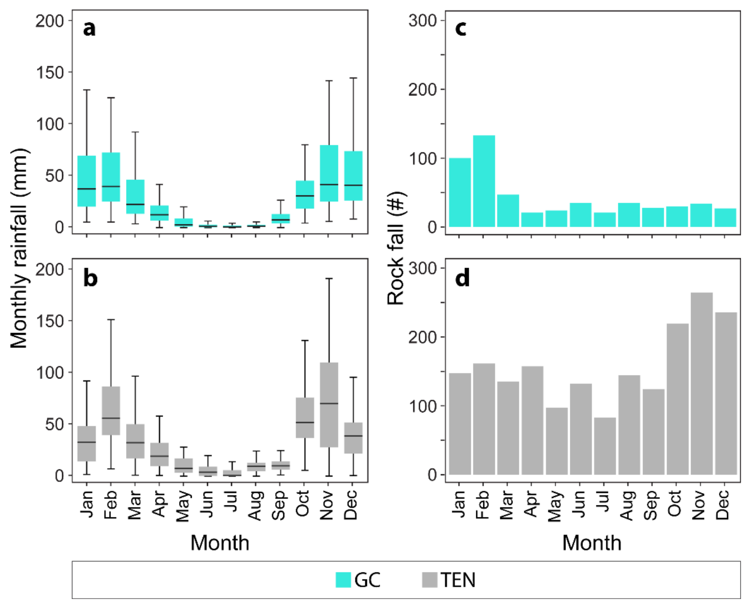

Figure 2. Comparison between monthly rainfall and rockfall occurrence. (a, b) Annual variation of monthly rainfall measures in GC (cyan) and TEN (grey). The whiskers show 1.5 times the interquartile range. (c, d) Number of rockfalls per month in the two test sites.

https://doi.org/10.5194/nhess-2020-111
Preprint. Discussion started: 21 April 2020

Natural Hazards and Earth System Sciences
Open Access
EGU
Discussions

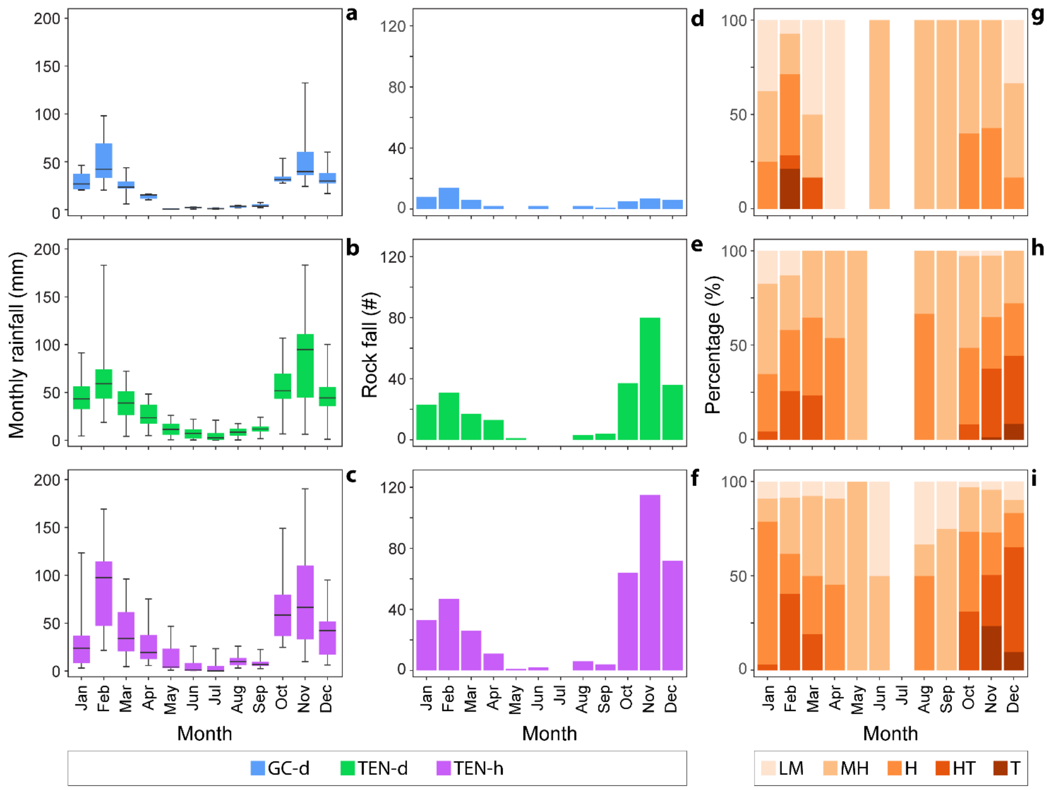

Figure 3. Comparison between monthly rainfall and rainfall-induced rockfalls and Alpert classification. (a, b, c) Annual variation of monthly rainfall measures in the test sites. Legend: GC-d, daily rainfall data in GC test site; TEN-d, daily rainfall data in the TEN test site; TEN-h, hourly rainfall data in TEN test site. (d, e, f) Number of rainfall-induced rockfalls per month. (g, h, i) Cumulated percentage of rainfall events per month classified according to Alpert et al. (2002). Legend: LM, light-moderate ($4 < E_d \leq 16$ mm); MH, moderate-heavy ($16 < E_d \leq 32$ mm); H, heavy ($32 < E_d \leq 64$ mm); HT, heavy-torrential ($64 < E_d \leq 128$ mm); T, torrential ($E_d > 128$ mm).

https://doi.org/10.5194/nhess-2020-111
Preprint. Discussion started: 21 April 2020

Natural Hazards and Earth System Sciences
Open Access
Discussions

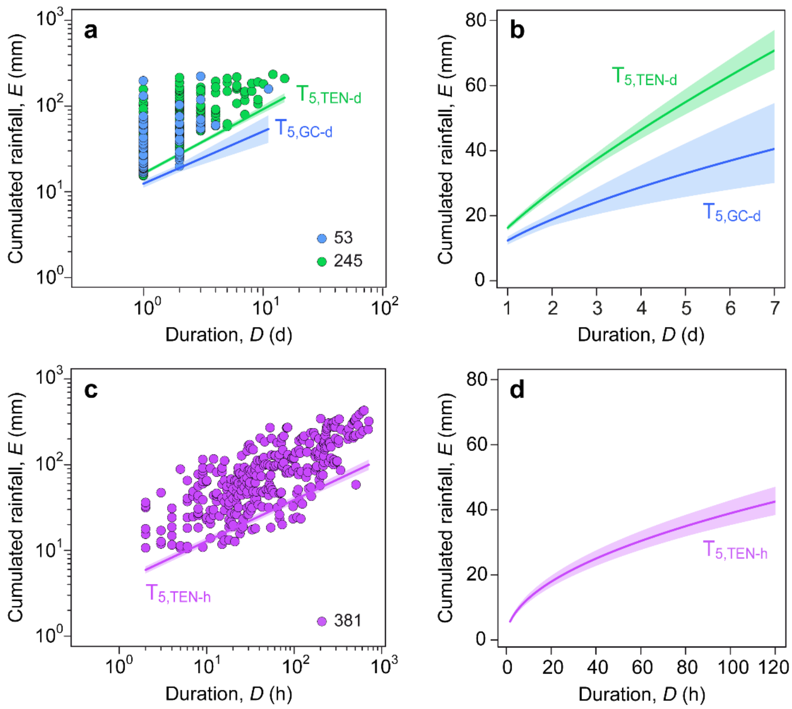

Figure 4. Rainfall thresholds for the possible rockfall occurrence in the two test sites. (a) Rainfall duration *D* (x-axis, in days) and cumulated event rainfall *E* (y-axis, in mm) conditions that have produced rockfalls in GC (53 blue dots) and TEN (245 green dots) test sites, respectively. Green and blue curves are the 5% power law thresholds ($T_{5,TEN\text{-}d}$, $T_{5,GC\text{-}d}$). (b) 5% daily *ED* thresholds for GC and TEN in linear coordinates, in the range of durations $1 \leq D \leq 7$ days. (c) Rainfall duration *D* (x-axis, in hours) and cumulated event rainfall *E* (y-axis, in mm) conditions that have produced rockfalls in TEN (381 purple dots) test site. Purple curve is the 5% power law threshold ($T_{5,TEN\text{-}h}$). (d) 5% hourly *ED* thresholds for GC and TEN in linear coordinates, in the range of durations $1 \leq D \leq 120$ hours.

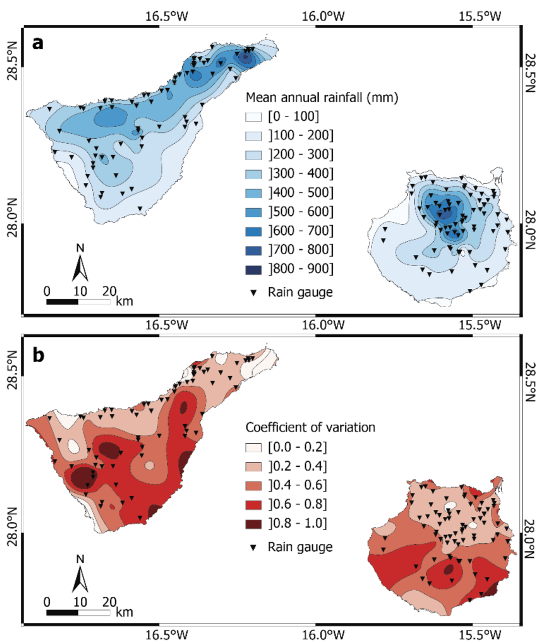

Figure 5. Maps of (a) mean annual rainfall and (b) of its coefficient of variation. The rain gauges used for these analysis (cf. Table 1) are also shown.

https://doi.org/10.5194/nhess-2020-111
Preprint. Discussion started: 21 April 2020

Natural Hazards and Earth System Sciences
Open Access
Discussions

Table 1. Summary of the three available rain gauge networks (CIAGC, AEMET, SIAR) in the two test sites (GC and TEN) i.e., network name, network operating time period, temporal resolution, test site, number of used rain gauges, their average operating time, and the use of data.

<table>
<tr><th>Network</th><th>Period</th><th>Temporal resolution</th><th>Test site</th><th>Rain gauges (#)</th><th>Average operating time (year)</th><th>Data application</th></tr>
<tr><td>CIAGC</td><td>Jan 2010 - Dec 2017</td><td rowspan="2">daily</td><td rowspan="2">GC</td><td>13</td><td>8.0</td><td rowspan="5">Thresholds</td></tr>
<tr><td rowspan="6">AEMET</td><td>Jan 1951 - May 2019</td><td>92</td><td>41.8</td></tr>
<tr><td>Oct 1997 - May 2019</td><td rowspan="2">hourly</td><td>GC</td><td>25</td><td>16.5</td></tr>
<tr><td>Jan 2010 - Mar 2018</td><td>TEN</td><td>34</td><td>5.5</td></tr>
<tr><td>Jan 2010 - May 2018</td><td>daily</td><td>TEN</td><td>66</td><td>8.2</td></tr>
<tr><td rowspan="2">Jan 2000 - Dec 2019</td><td rowspan="2">yearly</td><td>GC</td><td>67</td><td>15.2</td><td rowspan="4">MAR</td></tr>
<tr><td>TEN</td><td>58</td><td>13.8</td></tr>
<tr><td rowspan="2">SIAR</td><td rowspan="2">Jan 1999 - Dec 2019</td><td rowspan="2">monthly</td><td>GC</td><td>5</td><td>18.2</td></tr>
<tr><td>TEN</td><td>9</td><td>15.1</td></tr>
</table>

https://doi.org/10.5194/nhess-2020-111
Preprint. Discussion started: 21 April 2020

Natural Hazards and Earth System Sciences
Open Access
EGU
Discussions

Table 2. Summary of the number (#) and percentage (%) of MPRC in the categories proposed by Alpert et al. (2002), in the two test sites.

Category	E_d (mm)	GC-d		TEN-d		TEN-h	
		#	%	#	%	#	%
Light (L)	$E_d \leq 4$	0	0	0	0	0	0
Light-moderate (LM)	$4 < E_d \leq 16$	11	20.7	11	4.5	28	7.3
Moderate-heavy (MH)	$16 < E_d \leq 32$	23	43.4	92	37.5	86	22.6
Heavy (H)	$32 < E_d \leq 64$	14	26.4	80	32.7	117	30.7
Heavy-torrential (HT)	$64 < E_d \leq 128$	2	3.8	58	23.7	116	30.5
Torrential (T)	$E_d > 128$	3	5.7	4	1.6	34	8.9

532 Table 3. *ED* rainfall thresholds at different non-exceedance probabilities (1%, 5%, 10%, 20%, 35% and 50%)
533 for the GC and TEN test sites. The number of MPRC and the duration range of each threshold are also reported.

Threshold name	Number of MPRC	Threshold equation	Duration range
$T_{1,GC\text{-}d}$	53	$E = (8.3±1.0)×D^{(0.62±0.10)}$	1-11 days
$T_{5,GC\text{-}d}$		$E = (12.3±1.2)×D^{(0.62±0.10)}$	
$T_{10,GC\text{-}d}$		$E = (15.1±1.4)×D^{(0.62±0.10)}$	
$T_{20,GC\text{-}d}$		$E = (19.5±1.8)×D^{(0.62±0.10)}$	
$T_{35,GC\text{-}d}$		$E = (25.5±2.5)×D^{(0.62±0.10)}$	
$T_{50,GC\text{-}d}$		$E = (31.9±3.6)×D^{(0.62±0.10)}$	
$T_{1,TEN\text{-}d}$	245	$E = (11.6±0.6)×D^{(0.75±0.05)}$	1-15 days
$T_{5,TEN\text{-}d}$		$E = (16.3±0.8)×D^{(0.75±0.05)}$	
$T_{10,TEN\text{-}d}$		$E = (19.6±0.8)×D^{(0.75±0.05)}$	
$T_{20,TEN\text{-}d}$		$E = (24.4±1.0)×D^{(0.75±0.05)}$	
$T_{35,TEN\text{-}d}$		$E = (30.6±1.4)×D^{(0.75±0.05)}$	
$T_{50,TEN\text{-}d}$		$E = (37.1±1.8)×D^{(0.75±0.05)}$	
$T_{1,TEN\text{-}h}$	381	$E = (2.8±0.3)×D^{(0.48±0.02)}$	2-712 hours
$T_{5,TEN\text{-}h}$		$E = (4.3±0.4)×D^{(0.48±0.02)}$	
$T_{10,TEN\text{-}h}$		$E = (5.3±0.5)×D^{(0.48±0.02)}$	
$T_{20,TEN\text{-}h}$		$E = (6.9±0.6)×D^{(0.48±0.02)}$	
$T_{35,TEN\text{-}h}$		$E = (9.1±0.7)×D^{(0.48±0.02)}$	
$T_{50,TEN\text{-}h}$		$E = (11.4±1.0)×D^{(0.48±0.02)}$	

534